CrystEngComm

Accepted Manuscript

ROYAL SOCIETY OF CHEMISTRY

www.rsc.org/crystengcomm

Journal Name

RSCPublishing

ARTICLE

Large scale synthesis of gold dendritic nanostructures for surface enhanced Raman scattering

Cite this: DOI: 10.1039/x0xx00000x

Tianyu Xia,[ab] Hu Luo,[a] Shouguo Wang,[*b] Jialong Liu [a], Guanghua Yu [b] and Rongming Wang[*ab]

Received 00th January 2012,
Accepted 00th January 2012

DOI: 10.1039/x0xx00000x

www.rsc.org/

Large scale Au dendritic nanostructures with sharp tips have been successfully fabricated by reducing potassium tetrachloroaurate ($KAuCl_4$) with hydrofluoric acid on Si wafer locally processed by a focused ion beam (FIB) technique. The surface enhanced Raman scattering (SERS) with Rhodamine B (RhB) molecules on nanostructured substrate is greatly enhanced, originating from "hot-spots" located at the nanogaps between adjacent branches on dendritic nanostructures. Furthermore, Au dendritic nanostructures as a recyclable SERS substrate exhibit an ultrasensitive response to the pico-scale concentration of probe molecules. This work shows that greatly enhanced SERS substrates with a high degree of reliability and reproducibility can be fabricated at relative low cost, which could help SERS to realize its full potential as a very sensitive tool for trace analysis.

Introduction

Due to its extremely high sensitivity and nondestructive character in molecule detection, surface enhanced Raman scattering (SERS) has attracted much interest in molecular chemical information, surface science and environmental monitoring since the first observation in 1970s.[1-7] In general, two fundamentally different mechanisms dominate in SERS. One is the chemical enhancement caused by the charge transfer between the metal surface and adsorbed molecules. The other is the physical enhancement due to electromagnetic effect from the excitation of surface plasmon resonance (SPR) in noble metal nanostructures.[5-11] The electromagnetic effect is several orders larger in magnitude than that of chemical enhancement.[1, 5, 8, 9] Therefore, the "hot-spots" in metal substrate where strong electromagnetic fields appear plays a vital role in the enhancement of Raman signal. Kinds of substrates have been tried to increase the density, sensitivity, and reproducibility of "hot-spots" in order to produce the stronger SERS signal.[1, 2, 4-8]

The micro/nano-scale particles or thin films of Au, Ag and Cu have been widely accepted as efficient SERS substrates.[1] Furthermore, Au and Ag are more suitable for SERS applications as they can offer stronger plasmonic fields, together with excellent optical tenability and biocompatibility.[12] Although Ag has superior optical performance, its application is limited due to the poor oxidation resistance.[13] Two main methods have been developed to synthesize the SERS substrates, including the chemical reduction method and scanning beam lithography.[1-7, 9, 12] Although chemical reduction method is widely used, the chemically produced nanostructures are easily being capped by the surfactant which not only diminishes the intensity of SERS signal but also is unfriendly to environment.

With respect to scanning beam lithography, focused ion beam (FIB) technique has been proven to be a unique tool to fabricate nanostructures on a large scale. FIB is capable of precise control over the size, shape, and distribution of metallic nanostructures with well tunable optical properties, leading to a very high sensitivity in the SERS.[14] Various metallic nanostructures such as nanohole arrays, nanoflowers and nanoantennas were fabricated by FIB in the field of plasmonics.[14-16] Recently, a rapid process has been developed to fabricate the magnetic nanoneedle arrays.[17, 18] In this work, an easily prepared, reliable and environment-friendly method is proposed to produce high quality SERS substrates with controllable "hot-spots" located at the nanogaps in dendritic nanostructures. Locally patterned areas on Si wafer are fabricated by FIB and then Au dendritic nanostructures are formed on the patterned squares by the galvanic displacement reaction and diffusion-limited aggregation (DLA). Au dendritic nanostructures as a recyclable SERS substrate exhibit an ultrasensitive response to the low concentration ($\leq 10^{-12}$ M) of probe molecules, indicating that the FIB implantation is conducive to form SERS preferential structures.

Experimental details

Millimeter size Si pieces were cleaned ultrasonically in acetone, distilled water and ethanol in sequence. Consequently, thermal oxide layer was formed at 900 °C in the air to protect the undosed area. The local patterning was carried out at the FIB-SEM dual beam workstation (Strata, DB-235, FEI). The milling ion dose was about 4.0×10^{16} ions/cm^2 with the beam parameters of 30 keV acceleration voltage, 500 pA beam current, 1 μs dwell time and 50% overlap. The

* Corresponding author. E-mail: sgwang@ustb.edu.cn and rmwang@ustb.edu.cn
[a] Department of Physics, Beihang University, Beijing 100191, China
[b] University of Science and Technology Beijing, Beijing 100083, China.

patterned square was 20×20 μm^2 in size to ensure the total containing of Raman laser beam during Raman measurements. For comparison, another piece of Si wafer was cleaned, but without annealing and patterning.

Au nanostructures were grown on Si wafers via galvanic displacement reaction and DLA. The reaction solution was prepared with 1 mM $KAuCl_4$ and 6% HF in the distilled water. Two Si wafers with and without FIB patterned areas were dipped into the mixed reaction solution for 1 min at room temperature. Finally, the samples were rinsed with ethanol and quickly dried in an oven at 100 °C.

The SERS spectra were collected with the Renishaw in Raman microscopy. To evaluate the SERS property of Au nanostructures, RhB as probe molecules were dropped onto substrates and dried in the air for its established vibration features. The SERS active substrates were excited by the laser with 532 nm wavelength.

Results and discussion

In order to illustrate the significant influence of ion implantation by FIB on the formation of the formed Au dendritic nanostructures, a series of experiments were carried out with and without ion implantation under the same conditions. Before patterning, a piece of Si wafer was chemically treated in order to obtain a smooth and clean surface shown in inset of Fig. 1(a). After etching at room temperature, many discrete white dots appear on Si surface (inset in Fig. 1(c)). High-energy Ga^+ ions can break Si surface, leading to many active Si atoms. The white nanoclusters shown in inset in Fig. 1(c) are Si droplets formed as a result of energy deposition on the surface.[17] The related AFM image and roughness parameters are shown in Fig. S1 and Table S1, respectively.

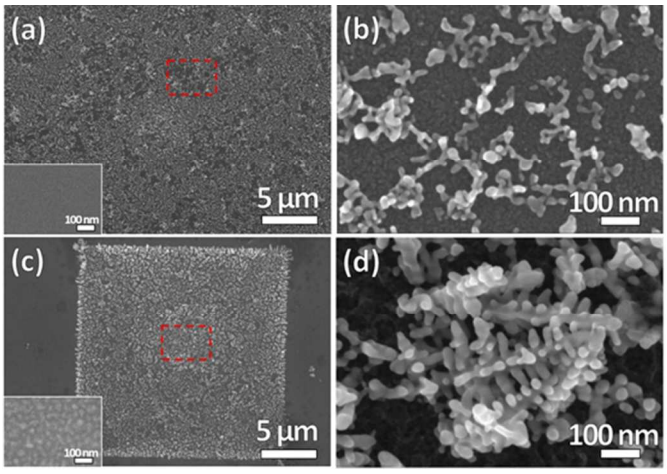

Fig. 1 SEM images for Au nanostructures after chemical reaction on Si wafer (a) without and (c) with Ga^+ ion implantation. The inset of (a) and (c) is SEM image of bare and patterned Si wafer, respectively. Panel (b) and (d) is high magnification image of the area shown by dashed box in (a) and (c), respectively.

Fig. 1(a) presents the SEM image of Au nanostructures grown on Si wafer without patterning. The nanostructures are earthworm-like, constructed by Au nanoparticles (about 20 nm in diameter) with the length of 100-300 nm. This shape can be seen more clearly by a higher magnification image shown in Fig. 1(b). Fig. 1(c) shows the SEM image of Au nanostructures grown on the patterned Si wafer. The bright image in the center is for patterned area, and the dark area is unpatterned surface, respectively. The bright and dark area comes from FIB etched layer and from the SiO_2 layer formed due to annealing, respectively. With respect to patterned area, Fig. 1(d) clearly shows well defined Au dendritic nanostructures along the backbone with branches. The branches extend at certain angles with respect to the backbone, with the length of about 300 nm and the diameter in a range of 30-50 nm. The length of the whole Au dendritic nanostructures is about 400 nm. Above results provide clear evidence that FIB ion implantation plays a significant role in the morphology control of Au nanostructures. The composition of the obtained samples was further studied by SEM mapping shown in Fig. S2.

The mechanism to form dendritic nanostructures on the patterned area is of great importance to enhance our understanding of their properties, including enhanced SERS signal and ultrahigh sensitivity molecular detection, which will be discussed later on. The galvanic displacement and DLA model will be used to explain the origin of above dendritic nanostructures. Fig. 2 schematically shows the formation process of Au dendritic nanostructures. Prior to FIB patterning, a protective SiO_2 layer (Fig. 2(b)) was formed on the clean Si wafer (Fig. 2(a)) due to annealing. As described previously, Si atoms segregate from the bulk with ion implantation, leading to Si islands in size of about 15 nm on the surface as shown in Fig. 2(c). These Si nanoislands could be more active compared with Si atoms in the wafer.

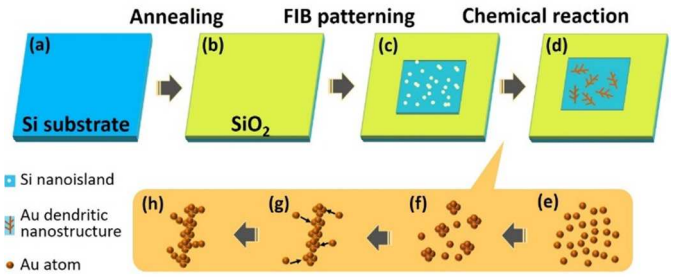

Fig. 2 Illustration for the process of Au dendritic nanostructures: clean Si wafer (a), SiO_2 layer (b), patterned area on Si wafer by FIB (c), Au dendritic nanostructures (d), and the process (e)~(h).

According to the galvanic displacement, the synthesis of Au nanostructures on Si surface comes from a sufficiently high oxidation potential of Au^{3+} ions, described by the equation (1) and (2) [19]

$$Si + 6F^- \rightarrow SiF_6^{2-} + 4e^- \quad E^o_{SiF_6^{2-}/Si} = -1.2\ V\ vs.\ NHE \qquad (1)$$

$$AuCl_4^- + 3e^- \rightarrow Au(s) + 4Cl^- \quad E^o_{Au^{3+}/Au} = +1.42\ V\ vs.\ NHE \qquad (2)$$

The displacement process is essentially a corrosion reaction in conjunction with Au deposition, where Si nanoparticles acting as a source of electrons to reduce Au^{3+} ions in the solution. As a result of this reaction, Si surface is spontaneously oxidized to dielectric SiO_2, which prevents further Au^{3+} reduction.[20] Since Au^{3+} reduction process is prohibited by SiO_2, this reaction will immediately stop after the formation of SiO_2. The addition of HF in the solution is to dissolve SiO_2 and locally form the soluble SiF_6^{2-}.[19, 20] Over a large number of trials, a proper concentration of HF was optimized, which can not only remove SiO_2 produced in the displacement reaction but also keep the oxidized layer during annealing.

The nonequilibrium system is crucial for the DLA model, which is generally used for the formation of Au dendritic nanostructures.[21] The active Si nanoislands have been reduced by Au^{3+} ions in priority, resulting in the nonequilibrium system. Furthermore, the implantation of high-energy Ga^+ ions destroys

Si wafer surface and many trenches are formed inside the Si wafer, which greatly increases the imbalance of reaction system. Accompanied by the reduction of Au^{3+} ions, a large quantity of Au atoms will then be formed at random positions on the Si wafer schematically shown in Fig. 2(e). Once the particle concentration reaches a critical value, these Au atoms aggregate to lager particles (Fig. 2(f)), forming the building blocks of the backbone subject to surface energy minimisation (Fig. 2(g)).[22, 23] There is a concentric diffusion field around the backbone [24,25]. In the present system, the subsequent Au atoms tend to attach to the backbone and create favorable sites for atomic accumulation due to optimal organisation (Fig. 2(g)).[22] The growth proceeds preferentially along the branches, and the self-assembling of Au dendritic nanostructures continues until the concentration of Au^{3+} ions decreases to a low level which cannot maintain the further reaction (Fig. 2(h)).

Compared with Au dendritic nanostructures, earthworm-like nanostructures are formed by galvanic displacement in HF solution randomly on another Si wafer without FIB patterning. The DLA process does not take place here because the Au nuclei are instantaneous, not as progressive as dendritic nanostructures. The possibility for surface Si atoms reacting with Au^{3+} ions is constant in the whole solution, leading to nuclei number rapidly to a certain value in an equilibrium system compared with the patterned Si wafer.[21] It should be noted that the DLA process develops only when the concentration of particles is low so that the aggregation is governed by diffusion.[26]

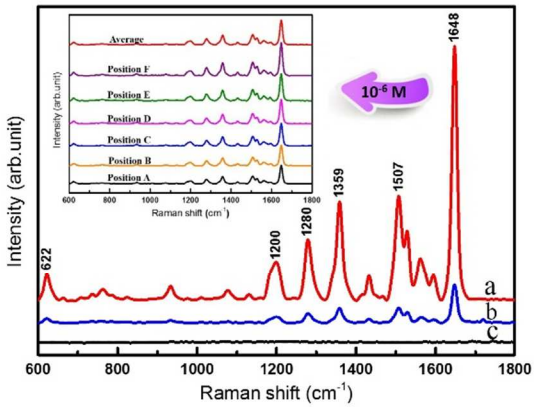

Fig. 3 Raman spectra of RhB on Au dendritic nanostructures (a), earthworm-like nanostructures (b) and Si wafer (c), where the concentration of RhB is 10^{-6} M and the laser wavelength is 532 nm, respectively. Inset: SERS spectra of RhB (10^{-6} mol/L) on Au dendritic nanostructures at six positions (Position A-F) and their average signals.

The SERS as a powerful tool to detect the chemical information of molecules on metal substrate surface has been explored actively because of its high sensitivity and reliable identification of molecular structures.[1, 2, 7] In order to check the SERS performance of above Au dendritic nanostructures, the RhB as probe molecules are dropped onto various substrates. As commonly used dye molecule, RhB is chosen as an analyte here because it has been well characterized by Raman spectrum. Fig. 3 shows the SERS spectra of RhB on Au dendritic nanostructures (a), on Au earthworm-like nanostructures (b) and on bare Si wafer (c), respectively, where the laser wavelength is 532 nm. The spectra were recorded under the same parameters, such as the volume of probe molecules (10^{-6} M), the exciting wavelength, and the laser power. From Fig. 3, the pronounced peaks located at 622, 1200, 1280, 1359, 1507 and 1648 cm^{-1} are observed, in good agreement with results from literature.[6] With respect to the spectra, three major bands at 1648, 1570 and 1359 cm^{-1} are attributed to the aromatic C-C stretching. In addition, the band at 1280, 1200 and 622 cm^{-1} originates from the C-C bridge-bands stretching, aromatic C-H bending and aromatic bending, respectively.

According to the general method of calculation,[27] the analytical enhancement factor (EF) for the substrate is estimated using the following formula

$$EF = \frac{I_{SERS}/N_{surf}}{I_{Raman}/N_{bulk}} \quad (3)$$

Where I_{SERS} and I_{Raman} denotes the intensity of a vibrational mode in SERS and Raman spectra, respectively. N_{bulk} and N_{surf} stands for the number of RhB molecules in bulk and adsorbed on substrate surface effectively excited by a laser beam, respectively. To calculate the EF for RhB absorbed on the surface of Au dendritic nanostructures, the Raman spectra of RhB dispersed on bare Si wafer was obtained under the same experimental conditions shown in Fig. S3. Then, the EF was estimated to be as high as 10^7 based on the intensity of the vibrational mode at 1648 cm^{-1}.

In general, the SERS signal is strongly dependent on the exterior morphology and surface structure of the substrate, including the distance, the shape, and the distribution of surface nanoparticles.[7, 8, 22] It has been proven that the nanogaps between particles play a predominant influence on SERS signals.[1, 7, 8, 28] When two nanoparticles are located at a certain distance (such as a few nanometers), the local electromagnetic fields in the nanogaps are greatly enhanced under the resonance conditions. This local area in nanometer size is called "hot-spots" for Raman scattering.[1, 7] Therefore, an effective SERS substrate requires an abundant of "hot-spots" with small gaps on the substrate surface.

Raman measurements were carried out in six different positions on the 20×20 μm^2 Si wafer in random, and their average spectra were presented in Fig. 3. SERS spectra of RhB (10^{-6} mol/L) on Au dendritic nanostructures at six different positions (Position A-F) and their average signals are shown in inset of Fig. 3. Sharp peaks with higher intensity are clearly observed in the SERS spectra of Au dendritic nanostructures as the substrate (indicated by a), compared with Au earthworm-like nanostructures (indicated by b) and Si wafer without any Au nanostructures (indicated by c). Two mechanisms could be involved in the enhanced SERS signals for Au dendritic nanostructures. Firstly, the SEM images shown in Fig. 1(d) indicate that well dispersed Au dendritic nanostructures consisted of numerous branches which symmetrically distribute on the backbone with nanogaps between adjacent branches in scale of 5-30 nm. The nanogaps between Au branches are so small, leading to the strong coupling among surface plasma of branches excited by the laser beam. Therefore, this successive resonance results in the amplification of the electromagnetic fields and Raman enhancement of adsorbed molecules.[1, 29, 30] Secondly, numerous nanogaps can not only afford high density of "hot-spots" but also can effectively trap RhB molecules in the "hot-spots" to generate the significant Raman enhancement.[22] The Raman signals of RhB are greatly enhanced in the district of strong localized plasma.

Although the Au earthworm-like nanostructures have SERS effect towards RhB, its intensity is lower than that of dendritic nanostrcutures. The weaker fields come from the lack of effective nanogaps in earthworm-like structures for SERS enhancement. Since surface structures can adjust the coupling

interaction of surface plasma, FIB patterning provides a powerful method to manipulate these Au nanostructures and in turn the SERS performance. Au dendritic nanostructures synthesized on Si wafer can be applied to fabricate highly effective SERS substrates at large scale because of their ability for electromagnetic field enhancement.

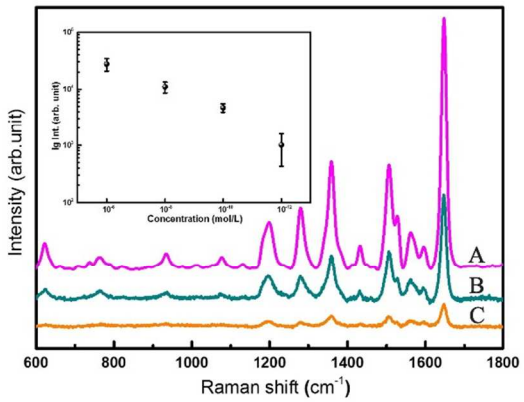

Fig. 4 The SERS with various RhB concentrations of 10^{-8} M (A), 10^{-10} M (B), 10^{-12} M (C), respectively, where the intensity of (C) is increased by 10 times for comparison. Inset: Intensities of the 1648 cm^{-1} band with different concentrations of RhB.

Based on the above discussion, it is reasonable to conclude that the optimized Au dendritic nanostructures on the patterned area by FIB can be used as potential candidates for SERS. In order to investigate the detection limit of probe molecule, the RhB solution with a series of concentration is tested by using Au dendritic nanostructures. Fig. 4 presents the SERS with various RhB concentrations of 10^{-8} M (A), 10^{-10} M (B), 10^{-12} M (C), respectively, where the intensity of (C) is increased by 10 times for clear comparison. The SERS intensity gradually decreases with decreasing the concentration of RhB with the laser wavelength of 532 nm. It is of great interest to find that when the concentration is further reduced to 10^{-12} M, the enhanced signals can still be obviously detected. This shows that Au dendritic nanostructures could act as promising candidates to detect the trace biomolecules or toxical chemicals.[22] The error bars are offered in inset of Fig. 4 to indicate intensities of the peaks in the figures and to estimate enhancement capability of the substrate. Such fluctuation and variation of the enhancement factor would play a neglectable effect on the integral SERS performance.

Furthermore, the stability of Au dendritic nanostructures as SERS substrate was examined. After 4 months stored at atmosphere conditions, their performance is nearly comparable with those from the fresh samples. Thus, the result shows that the sample has a good reproducibility, providing a wider use such as in the molecular detection.

Conclusions

In summary, a precisely controlled FIB technique is used to fabricate Au dendritic nanostructure on a large scale. The growth mechanism model based on the galvanic displacement and DLA is proposed to explain the controlled synthesis of Au dendritic nanostructures. These Au dendritic nanostructures exhibit excellent SERS properties with a low concentration RhB as the target molecule and the enhancement factor of SERS reaches 10^7. In addition, the Au dendritic nanostructures as SERS substrate also have superior sensitivity and stability. Based on the outstanding performance of Raman, Au dendritic nanostructures could find wide applications in the biosensing, biochemistry analysis, chemical production and environmental monitoring fields.

Acknowledgements

This work was supported by the Natural Science Foundation of China (Nos. 51371015, 51431009, 51471183, 51331002 and 11274371) and the Fundamental Research Funds for the Central Universities (230201406500013).

References

1. Y. Sun, K. Liu, J. Miao, Z. Wang, B. Tian, L. Zhang, Q. Li, S. Fan and K. Jiang, *Nano Letters*, 2010, **10**, 1747-1753.
2. S. Lee, M. G. Hahm, R. Vajtai, D. P. Hashim, T. Thurakitseree, A. C. Chipara, P. M. Ajayan and J. H. Hafner, *Advanced Materials*, 2012, **24**, 5261-5266.
3. Y. Li, X. Qi, C. Lei, Q. Yue and S. Zhang, *Chemical Communications*, 2014, **50**, 9907-9909.
4. M. Hardy, M. D. Doherty, I. Krstev, K. Maier, T. Moller, G. Mueller and P. Dawson, *Analytical Chemistry*, 2014, **86**, 9006-9012.
5. A. Martin, A. Pescaglini, C. Schopf, V. Scardaci, R. Coull, L. Byrne and D. Iacopino, *Journal of Physical Chemistry C*, 2014, **118**, 13260-13267.
6. J. T. Zhang, X. L. Li, X. M. Sun and Y. D. Li, *Journal of Physical Chemistry B*, 2005, **109**, 12544-12548.
7. S. J. Lee, A. R. Morrill and M. Moskovits, *Journal of the American Chemical Society*, 2006, **128**, 2200-2201.
8. H. X. Xu, J. Aizpurua, M. Kall and P. Apell, *Physical Review E*, 2000, **62**, 4318-4324.
9. A. Campion and P. Kambhampati, *Chemical Society Reviews*, 1998, **27**, 241-250.
10. H. Xu, E. J. Bjerneld, M. Käll and L. Börjesson, *Physical Review Letters*, 1999, **83**, 4357-4360.
11. H. Wei and H. Xu, *Nanoscale*, 2013, **5**, 10794-10805.
12. A. M. Schwartzberg and J. Z. Zhang, *Journal of Physical Chemistry C*, 2008, **112**, 10323-10337.
13. Y. H. Jang, K. Chung, L. N. Quan, B. Spackova, H. Sipova, S. Moon, W. J. Cho, H.-Y. Shin, Y. J. Jang, J.-E. Lee, S. T. Kochuveedu, M. J. Yoon, J. Kim, S. Yoon, J. K. Kim, D. Kim, J. Homola and D. H. Kim, *Nanoscale*, 2013, **5**, 12261-12271.
14. M. Fan, G. F. S. Andrade and A. G. Brolo, *Analytica Chimica Acta*, 2011, **693**, 7-25.
15. H. Luo, R. Wang, Y. Chen, D. Fox, R. O'Connell, J. J. Wang and H. Zhang, *Crystengcomm*, 2013, **15**, 10116-10122.
16. H. Kollmann, X. Piao, M. Esmann, S. F. Becker, D. Hou, C. Huynh, L.-O. Kautschor, G. Boesker, H. Vieker, A. Beyer, A. Goelzhaeuser, N. Park, R. Vogelgesang, M. Silies and C. Lienau, *Nano Letters*, 2014, **14**, 4778-4784.
17. Y. Z. Huang, S. G. Wang, C. Wang, Z. B. Xie, D. J. H. Cockayne and R. C. C. Ward, *Applied Physics Letters*, 2006, **88**, 103104.
18. Y.-Z. Huang, D. J. H. Cockayne, J. Ana-Vanessa, R. P. Cowburn, S.-G. Wang and R. C. C. Ward, *Nanotechnology*, 2008, **19**, 015303.
19. S. Y. Sayed, F. Wang, M. Mallac, A. Meldrum, R. F. Egerton and J. M. Buriak, *Acs Nano*, 2009, **3**, 2809-2817.
20. A. Benkouider, A. Ronda, A. Gouye, C. Herrier, L. Favre, D. J. Lockwood, N. L. Rowell, A. Delobbe, P. Sudraud and I. Berbezier, *Nanotechnology*, 2014, **25**, 335303.
21. W. Ye, J. Yan, Q. Ye and F. Zhou, *Journal of Physical Chemistry C*, 2010, **114**, 15617-15624.
22. Y. Zhang, S. Sun, X. Zhang, L. Tang, X. Song and Z. Yang, *Physical Chemistry Chemical Physics*, 2014, **16**, 18918-18925.
23. R. M. Brady and R. C. Ball, *Nature*, 1984, **309**, 225-229.
24. J. Xu and D. Xue, *Journal of Physical Chemistry B*, 2006, **110**, 11232-11236.
25. Y. Zhang, S. Sun, X. Zhang, L. Tang, X. Song, B. Ding and Z. Yang, *Chemical Engineering Journal*, 2014, **240**, 494-502.
26. B. Lim and Y. Xia, *Angewandte Chemie-International Edition*, 2011, **50**, 76-85.

27. W. B. Cai, B. Ren, X. Q. Li, C. X. She, F. M. Liu, X. W. Cai and Z. Q. Tian, *Surface Science*, 1998, **406**, 9-22.
28. H. Chu, J. Wang, L. Ding, D. Yuan, Y. Zhang, J. Liu and Y. Li, *Journal of the American Chemical Society*, 2009, **131**, 14310-14316.
29. J. C. Tsang, J. R. Kirtley and J. A. Bradley, *Physical Review Letters*, 1979, **43**, 772-775.
30. M. Fleischmann, Z. Q. Tian and L. J. Li, *Journal of Electroanalytical Chemistry*, 1987, **217**, 397-410.

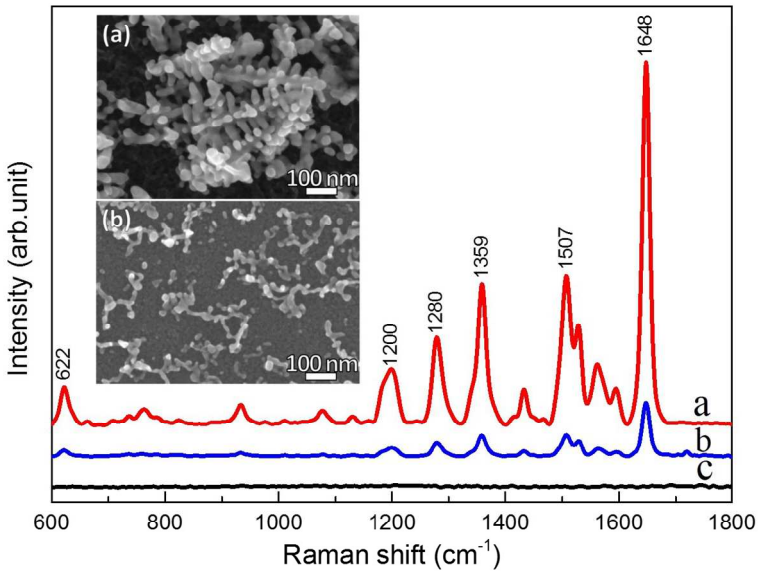

A precisely controlled FIB technique is used to fabricate Au dendritic nanostructure on a large scale. These Au dendritic nanostructures exhibit excellent SERS properties with a low concentration RhB as the target molecule and the enhancement factor of SERS reaches 107.
288x200mm (150 x 150 DPI)